

Calibration of the CLAIR Model by Using Landsat 8 Surface Reflectance Higher-Level Data and MODIS Leaf Area Index Products

Giuseppe Pescechera, Antonio Novelli^(✉) , Grazia Caradonna ,
and Umberto Fratino 

Politecnico di Bari, via Orabona 7, 70125 Bari, Italy

pescechera.g@gmail.com,

{antonio.novelli, grazia.caradonna, umberto.fratino}@poliba.it

Abstract. This study proposes a method for the calibration of the semi-empirical CLAIR model, a simplified reflectance model used to estimate Leaf Area Index (LAI) from optical data. The procedure can be applied in case of lacking of both LAI field measurements and surface reflectance data by exploiting free of charge data as the novel high level Landsat 8 Operational Land Imager Surface Reflectance (OLISR) product and the MODIS LAI (MCD15A3H level 4 product). This last dataset was used as LAI reference within an iterative procedure based on the resampling, at the MODIS pixel size, of LAI estimated from OLISR data. The procedure generated LAI information consistent with the MCD15A3H LAI estimation. Lastly, the method was tested and statistically assessed in a territory characterized by an extremely heterogeneous and fragmented landscape (irrigation district “Sinistra Ofanto”) located in the Apulia Region (Italy).

Keywords: Leaf Area Index · CLAIR model · Landsat 8 surface reflectance higher-level data · MCD15A3H

1 Introduction

Leaf Area Index (LAI) is defined as the one half of the total leaf area per unit ground area [1] and is a key parameter implemented in a large variety of climate, ecological and agricultural applications [2]. In particular, LAI is used as input parameter in many biophysical models for calculating vegetation parameters as evapotranspiration (e.g. [3, 4]) and net primary production (e.g. [5]).

Direct measurements of LAI over large areas require continuous updates and can be extremely time-consuming and not cost-effective owing to its large spatial and temporal variability [6]. This is especially true over heterogeneous landscapes [7] in which the analysis of spatial/temporal data is required [8]. In these cases, passive remotely sensed observations covering the visible to shortwave infrared (SWIR) spectral region are a valid alternative to provide a rapid and non-destructive LAI estimation [9]. Several algorithms were developed during

the past decades to estimate LAI from remote sensing. The procedures can be divided in four groups [10]: parametric regressions, non-parametric regressions, physical based approaches and hybrid methods. Parametric methods (e.g. [11]) assume an explicit relationship between LAI and spectral observations (typically a vegetation index) through a fitting function built by relying on statistical or physical knowledge of the variable and the spectral response. Among parametric methods, in this study was selected the semi-empirical CLAIR model (Clevers leaf area index by reflectance) [12]. The model estimates LAI of green canopy (vegetative stage) by means of an empirical logarithmic relationship of the Weighted Difference Vegetation Index (WDVI) [13]. Due to the WDVI, the model can compensate the errors related to soil background reflectance contribute [14].

CLAIR model LAI estimation requires the soil-line slope value to calculate the WVDI and to calibrate its own parameters: the asymptotic value of WDVI ($WDVI_{\infty}$) and the extinction and scattering coefficient (α). Although these parameters have a physical nature, they are estimated empirically from a set of LAI field measures [9, 15–17]. However, this practice requires special attention since field-measured and remote sensing data are different both in spatial resolution and accuracy [18, 19]. In case of lacking LAI and surface reflectance field measurements, the retrieval of model parameters could be performed collecting previous results (e.g. [20–22]). This solution is hardly applicable because of a very great number of soil and crop type combinations with respect to the number of produced works. Nevertheless, for its easy conception, the CLAIR model is still utilized in many studies (e.g. [23–26]).

Image-based estimation of the model parameters can be useful to extend the applications of the CLAIR model, especially lacking *in situ* measurements. Literature has already shown that the soil-line slope can be retrieved from surface reflectance images [27] and used to estimate vegetation biophysical parameters or soil surface status [28]. With regard to the $WDVI_{\infty}$, image-based solutions assume it as the maximum WDVI value for vegetated areas retrieved within an image (e.g. [9, 16, 29, 30]). In this way, it is possible to estimate LAI in all the images. To filter out outliers, Akdim et al. [31] proposed $WDVI_{\infty}$ estimation from WDVI time series, as a linear combination of their mean value and the standard deviation retrieved in each image.

The extinction coefficient requires crop specific calibration [9] because it describes the canopy architecture and depends on the crop type and the corresponding Leaf Angle Distribution (LAD) value. Vuolo et al. [16] tested a procedure to derive site-specific values of α and $WDVI_{\infty}$ for two study areas in Italy and Austria. However, this solution partially solved the problem because each new test site needs field LAI measurements to infer α . Once calibrated, the model could be applied to the newly images without the need of new field measurements.

The main goal of this work is to define a procedure for the evaluation of the two parameters of CLAIR model using only surface reflectance and LAI retrieved from satellite data. The method exploits only free of charge data. In this way is

possible to estimate LAI without expensive *in situ* measurements and satellite data acquisition.

For this purpose, Landsat 8 Operational Land Imager Surface Reflectance (OLISR) sensor data and the four days composite MODIS (Moderate Resolution Imaging Spectroradiometer) LAI products (MCD15A3H) were selected. In particular, Landsat 8 OLI datasets were used to implement the CLAIR model by applying different algorithms to perform the atmospheric correction (e.g. [15, 31, 32]).

The proposed procedure generates LAI information consistent with the MODIS LAI product and characterized by a higher resolution. The featured geometric resolution is the same of the surface reflectance data used as input in the CLAIR model. The procedure does not require the knowledge of the crop species present in the considered area. In fact, by taking in account the mixture of all crop types, the estimated parameters can be considered site specific (and not crop specific). Lastly, the procedure was tested and statistically assessed in a study area located in the Apulia Region (Italy) and characterized by an extremely heterogeneous and fragmented landscape.

2 Study Area and Data

The study area (Fig. 1) falls within the Italian irrigation district “Sinistra Ofanto”, a large cultivated area, characterized by an extremely heterogeneous landscape with the presence of vineyards, olive trees, orchards and cereals. The district is situated in the North of the Apulian Region and is delimited by the Ofanto river at the southeast and characterized by a typical Mediterranean climate with strong seasonal and inter-annual variability. The climate is semi-arid and the irrigation system (managed by the Consortium Capitanata) implements both reservoir and groundwater as often happens in other semi-arid Mediterranean regions (e.g. [33, 34]). For this study Landsat 8 OLISR and MODIS LAI (MCD15A3H) product acquired in the 2013 crop year were used. Both datasets were retrieved from the U.S. Geological Survey (USGS) archives (<https://earthexplorer.usgs.gov/>). Landsat 8 OLISR data are developed for supporting land surface change studies. OLISR products include: Original Input Products (Level-1 data files, Quality Assessment Band file and meta-data text file), Top of Atmosphere (TOA) Reflectance, Surface Reflectance (SR), Brightness Temperature products and Surface Reflectance-based Spectral Indices (such as NDVI, NDMI, NBR, SAVI, EVI). These data are obtained with the algorithm Landsat 8 Surface Reflectance Code (LaSRC). Although LaSRC is a new algorithm (that should be considered provisional), the first test carried out showed that the LaSRC OLISR product performed better than previous LEDAPS (Landsat Ecosystem Disturbance Adaptive Processing System) products [35]. This result was achieved by using the coastal aerosol band and auxiliary climate data from MODIS for the implementation of the radiative transfer model. OLISR products have inherited the properties of the previous Landsat 8 products: 30-meter spatial resolution with a 16-day temporal

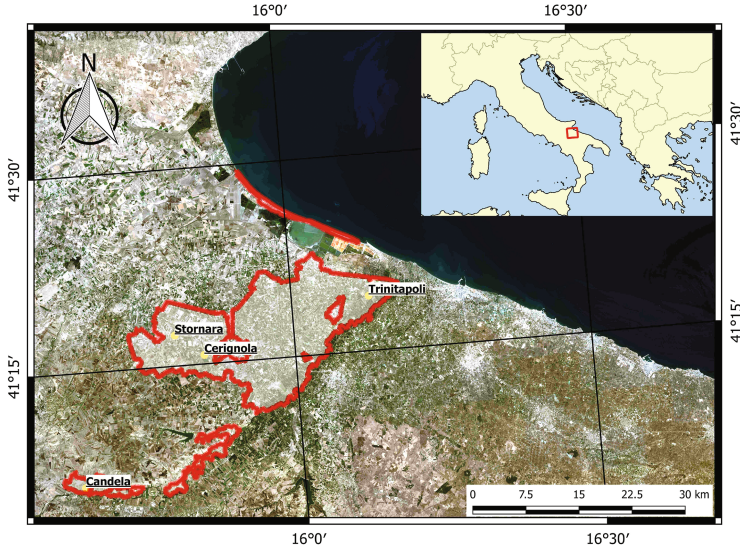


Fig. 1. The irrigation district “Sinistra Ofanto” (North of the Apulian Region Italy) as seen by a true color visualization of Landsat 8 (7 August 2013 - Reference System WGS 84).

resolution [36]. Further details related to the Landsat 8 OLISR product (e.g. data type, data range, correction coefficients, etc.) can be found in the “Provisional Landsat 8 surface reflectance code (LASRC)” (<https://landsat.usgs.gov/landsat-surface-reflectance-high-level-data-products>) product guide.

The site-specific CLAIR calibration was executed using the Cloud mask band (CFmask) and the surface reflectance Blue (Band 2), Green (Band 3), Red (Band 4) and Near Infrared (NIR - Band 5) bands. Moreover, the study area is included in two Landsat 8 frames, named by the notation Path-Row 189-031 and 188-031 of Landsat 8 Pre-Worldwide Reference System (WRS-2). The satellite acquisitions in these two frames are shifted by 7/9 days. For this reason, the temporal resolution of surface reflectance data for the study area is nearly doubled. In this study eleven Landsat 8 OLISR images, acquired from 05/19/2013 to 11/02/2013 without cloud contamination over the study area, were used. The complete scene list is reported in the Table 1.

The product MCD15A3H (level 4) is included in the latest version of MODIS LAI and Fraction of Photosynthetically Active Radiation (FPAR) products, Collection 6 (C6). It was derived from the combined use of Terra and Aqua satellite and generated with 500-meter spatial resolution and a temporal compositing period of 4 days. As remarked by Gao et al. using a four-day composite product can ensure a better temporal product, particularly during the period of rapid crop growth [2]. MCD15A3H data include 6 Science Dataset: LAI and FPAR with their standard deviation (LAI_500m, Fpar_500m, LaiStdDev_500m, FparStdDev_500m) and two quality assessment bands at the pixel level (FparLai_QC,

Table 1. Available Landsat 8 surface reflectance scenes and MCD15A3H LAI (M LAI) products over the study area for the 2013 crop year.

Landsat 8 OLISR			Prev. M LAI		Next M LAI	
Date	DOY	Path-Row	Date	DOY	Date	DOY
05/19/13	139	188 - 031	05/17/13	137	05/23/13	141
06/20/13	171	188 - 031	06/18/13	169	06/24/13	173
07/13/13	194	189 - 031	07/12/13	193	07/17/13	197
07/29/13	210	189 - 031	07/28/13	209	08/02/13	213
08/07/13	219	188 - 031	08/05/13	217	08/11/13	221
08/14/13	226	189 - 031	08/13/13	225	08/18/13	229
08/23/13	235	188 - 031	08/21/13	233	08/27/13	237
09/08/13	251	188 - 031	09/06/13	249	09/12/13	253
09/24/13	267	188 - 031	09/22/13	265	09/28/13	269
10/26/13	299	188 - 031	10/24/13	297	10/30/13	301
11/02/13	306	189 - 031	11/01/13	305	11/06/13	309

FparExtra_QC). The MODIS LAI algorithm consists of a main Look-Up-Table (LUT) based procedure. The LUT was generated using the 3D radiative transfer equation [37] and exploits the spectral information content of the MODIS red and NIR surface reflectance. When the LUT method fails, the algorithm utilizes the backup method based on empirical relationships between LAI and the Normalized Difference Vegetation Index (NDVI). Yang [38] demonstrated that the best quality is obtained from the main algorithm.

Among the datasets stored in the MCD15A3H product the following layers were used in this study: LAI (Lai_500m); Quality Control information band (FparLai_QC) that specifies the overall quality of the product (algorithm path and quality of the input data); Standard Deviation (LaiStdDev_500m) related to the uncertainty in the estimation of LAI. To consider LAI data close to the acquisition of the surface reflectance, for each Landsat surface reflectance data the previous and the successive MCD15A3H data were considered, as reported in Table 1.

3 Method

The semi-empirical CLAIR model (Eq. 1) is based on a simplified reflectance model that exploits an empirical logarithmic relationship between LAI and WDV I [13]:

$$LAI = - \left(\frac{1}{\alpha} \right) * \log \left(1 - \frac{WDVI}{WDVI_{\infty}} \right) \quad (1)$$

WDVI is a vegetation index developed to consider the influence of soil background reflectance [14]. The WDV I (Eq. 2) is defined as a weighted difference

between the measured NIR and Red reflectance (respectively ρ_{NIR} and ρ_{Red}) assuming as weighting factor the “soil-line slope” (a) defined (Eq. 3) as the ratio between NIR and red reflectance of bare soil ($\rho_{NIR,s}$, $\rho_{Red,s}$):

$$WDVI = \rho_{NIR} - (a * \rho_{Red}) \quad (2)$$

$$a = \frac{\rho_{NIR,s}}{\rho_{Red,s}} \quad (3)$$

In the next sections are described the image-based procedure proposed for the retrieval of the soil-line slope (a), necessary to calculate the WDVI, and the parameters of the model ($WDVI_{\infty}$ and α) for the selected study area.

3.1 Identification of the Soil-Line Slope (a) and Asymptotical Limiting Value of WDVI ($WDVI_{\infty}$)

The evaluation of the soil-line slope started from the selection of a Region Of Interest (ROI) corresponding to bare soil. This operation was performed for each surface reflectance image due to the variability of the land cover during the vegetative season. The selection was conducted by exploiting “natural color” (Red-Green-Blue) and “false color” (NIR-Red-Green) band combinations. In addition, an NDVI thresholding filter was applied. In this way the pixels wrongly interpreted as bare soil and with NDVI value major than 0.20 corresponding to shrub and grassland were eliminated from the ROI [39]. From each bare-soil ROIs, the scatter plot between Red and NIR surface reflectance was calculated: the value of soil-line slope, for the selected scene and accordingly to Eq. 3, was assumed equal to the angular coefficient of the fitting line of the scatter plot. For the CLAIR model, the soil-line slope of the study area does not depend from the soil water content and thus it was calculated as the mean value of all the retrieved ones.

As stated within the “Introduction” section, in image-based estimation the $WDVI_{\infty}$ is often equal to the maximum WDVI value found within the scene. In this way, LAI can be estimated since the argument of the logarithm in Eq. 1 results greater than zero. The respect of this condition is necessary to ensure future applications of the model to the newly images. For this reason, $WDVI_{\infty}$ was estimated by increasing of the 6% the greatest WDVI value retrieved among all the surface reflectance scenes. This assumption was a consequence of empirical and iterative tests and reduced the problem of LAI saturation when WDVI values approach $WDVI_{\infty}$.

3.2 Extinction Coefficient (α)

The calibration of the extinction requires a preliminary pre-processing phase of the MODIS LAI data to retrieve LAI values, with the best quality and the lowest uncertainty, close to the acquisition of the surface reflectance. In this phase, for each Landsat surface reflectance data, the previous and the successive MCD15A3H data were considered. The elaborations, proposed in this paper, were applied for each MODIS pixel of the study area, following the 3 steps:

- Selection of the pixels with overall good quality: LAI retrieved using the main algorithm and without index saturation and presence of significant clouds. This information was carried out by the layer Quality Control (FparLai.QC).
- Among the selected pixels, were selected the pixels with the minor uncertainty in the estimation of LAI. This selection was carried out using the Standard Deviation data (LaiStdDev_500m) and excluding pixels with ratio StdDev/LAI major than 0.25.
- Lastly, LAI data close to the acquisition of surface reflectance data were calculated as mean values, among the previous and the successive MODIS LAI data, and only for the pixels common for both the MCD15A3H scenes. In this way, a further quality selection of the data was performed. It was considered the mean value since surface reflectance data occurred in the middle of two MODIS acquisitions.

The procedure proposed for the calibration of the extinction coefficient (α) is based on a simple method, proposed by Gao et al. [2], to retrieve LAI from Landsat using MODIS LAI products as reference. They proposed two different solutions to match coarse-resolution MODIS LAI data: one is to first aggregate the Landsat surface reflectance (SR) to MODIS resolution and then compute LAI at that scale; another way is to compute LAI from Landsat data and then linearly aggregate these fine-scale LAI value to the MODIS resolution. This last solution was adopted in the proposed method in which for each MODIS pixel the Landsat LAI was aggregated following Eq. 4:

$$LAI_{MODIS} = \frac{\sum_{i=1}^n LAI_{Land,i}(\alpha)}{n} = \frac{\sum_{i=1}^n f(SR_{Land,i}(\alpha))}{n} \quad (4)$$

Where f is the CLAIR model function (Eq. 1), i is the index associated with each Landsat pixel within a given MODIS pixel cell and n is the total number of Landsat pixels in the considered MODIS pixel cell.

The objective function (Eq. 5) of the iterative procedure is based on the difference between LAI MODIS and the LAI Landsat aggregate at the MODIS resolution, accordingly the previous equation. For each MODIS pixel (j), the objective function is shown in Eq. 5.

$$LAI_{diff,j}(\alpha) = LAI_{MODIS_{QC,i}} - \frac{\sum_{i=1}^n LAI_{Land,i}(\alpha, W DVI_{\infty}, W DVI_i)}{n} \quad (5)$$

For the Landsat pixels with W DVI values negative, it was assumed LAI ($LAI_{Land,j}$) equal to 0 because in these cases the LAI retrieved with the CLAIR model is negative and therefor without physical meaning. The possible range of α values was extended from 0.10 to 0.80 with steps of calculation of 0.025.

The range of α values was selected by analyzing previous ones retrieved in literature and estimated by means of regression analysis between computed LAI and field LAI measurements. These results are synthetically reported in Table 2.

In this case, the selected test range was greater than the previous ones to extend the investigations with respect to similar studies. For each scene was selected the value of the α parameter that determines the minor Mean Absolute

Table 2. Soil-line slope, maximum WDVl and extinction coefficient for the CLAIR model retrieved in literature. Parameters were estimated by using field measurements of LAI and surface reflectance.

Reference	Soil-line slope (a)	WDVI $_{\infty}$	Extinction coefficient (α)
Vannino et al. [32]	-	0.55	0.39 (0.34–0.70)
Akdim et al. [31]	1.02–1.25	0.40–0.51	0.37
Vuolo et al. [16]	1.47 (1.41–1.64)	0.60 (0.57–0.61)	0.34
	1.35 (1.24–1.42)	0.52 (0.47–0.59)	0.35
Richter et al. [9]	1.2	0.50	0.8
Minacapilli et al. [25]	-	0.57	0.225 (0.120–0.515)
Vuolo et al. [24]	0.90–1.10	0.64–0.68	0.40–0.47
DURso et al. [40]	0.97–1.16	0.51 (0.45–0.54)	0.42 (0.34–0.54)
Clevers et al. [23]	-	0.579 0.686	0.25–0.53

Difference (MAD (6)) computed between α Landsat retrievals, resampled at the MODIS resolution, and MODIS LAI products. MAD was calculated over the MODIS grid.

$$MAD = \frac{\sum_{j=1}^m LAI_{diff,j}(\alpha)}{m} \quad (6)$$

where m is the total number of MODIS pixels used for the calibration procedure.

Lastly, the α value (valid for the whole crop season) was calculated as the average value of the extinction coefficients retrieved among all the surface reflectance scenes.

4 Results and Discussion

The CLAIR model parameters for each image were retrieved following the procedure described in the last sections. Table 3 resumes the results of the calibration.

The soil-line slope values retrieved during the season were between 1.22 and 1.38 with an average value of 1.31. This range of values results in line with previous similar scientific studies (Table 3).

With the computed soil-line slope value, it was possible to calculate the WDVl for the study area and for each image. This operation was carried out both using the mean seasonal soil-slope (a_{mean} , see Table 3) and the image specific soil-slope values (a_i , see Table 3) with the purpose to estimate the difference in the maximum WDVl retrieved. The differences were not significant since in both the cases the maximum WDVl retrieved ($WDVI_{MAX}$), within the study area, was equal to 0.61. This result is in line with the values retrieved in literature as reported in Table 2. Vanino et al. [32], retrieved WDVl value of 0.55 for a vineyard situated within the irrigation district Sinistra Ofanto. However, this value was crop specific and was calculated to create a correspondence of pixels with maximum vegetation cover. In order to ensure future applications of the

Table 3. Soil-line slope, maximum WDV_I and extinction coefficient values retrieved for each satellite image in the study area using the proposed image-based method. For each scene, the maximum WDV_I was retrieved both using the corresponding soil-line slope ($f(a_i)$) and the seasonal mean soil-line slope value ($f(a_{mean})$).

Soil-line slope		WDV _I _{MAX}		Extinction coefficient (α)				
n. pixel				n. pixel	WDV _I _∞ = 0.61		WDV _I _∞ = 0.65	
ROI	a_i	$f(a_{mean})$	$f(a_i)$	LAI reference	α	MAD	α	MAD
267	1.22	0.44	0.45	967	0.33	0.18	0.31	0.18
477	1.40	0.61	0.61	1287	0.38	0.26	0.35	0.26
265	1.38	0.57	0.56	1096	0.35	0.30	0.32	0.29
269	1.29	0.51	0.51	1285	0.33	0.27	0.30	0.27
950	1.36	0.57	0.57	1299	0.37	0.26	0.34	0.26
770	1.34	0.55	0.55	1258	0.34	0.26	0.32	0.26
1282	1.28	0.54	0.55	1177	0.37	0.24	0.34	0.24
1315	1.24	0.52	0.52	1172	0.34	0.24	0.32	0.23
3838	1.27	0.55	0.55	1269	0.37	0.23	0.34	0.22
1522	1.30	0.60	0.60	687	0.39	0.15	0.37	0.15
2012	1.37	0.56	0.56	426	0.37	0.12	0.35	0.12
mean	1.31				0.36	0.23	0.33	0.291
max		0.61	0.61					

model to the newly images, WDV_I_∞ was estimated by increasing of the 6% the greatest WDV_I value retrieved among all the surface reflectance scenes. Therefore WDV_I_∞ was assumed equal to 0.65.

The calibration of the extinction coefficient, achieved adopting the proposed iterative procedure, was executed after the soil-slope and the WDV_I_∞ retrieval. The results depicted that the calibrated CLAIR is able to produce LAI values consistent with MODIS data. The maximum MAD value retrieved along all the scenes was equal to 0.29 (Table 3). The MAD was close to the range of MODIS LAI accuracy reported in the Standard Deviation layer, being the possible MODIS LAI standard deviations errors variable from 0 to 1 for LAI values included in the range 0–4. The scatterplots between the LAI MODIS (reference) and the LAI Landsat (Fig. 2), shows that the model tends to underestimate LAI. This is more evident for higher LAI values (greater than 2).

In order to verify the effects of the hypothesis adopted for the estimation of WDV_I_∞, the calibration procedure was iterated also with WDV_I_∞ equal to the mean value of WDV_I_{MAX} (0.61). In both cases the estimated extinction coefficient values are included in the range value found in literature (Table 2). It is important to underline that an increment of the 6% of the WDV_I_∞ value corresponds, for each scene, to a mean reduction of the 8% of the α values. The overall MAD values retrieved were very similar for the two parameter sets.

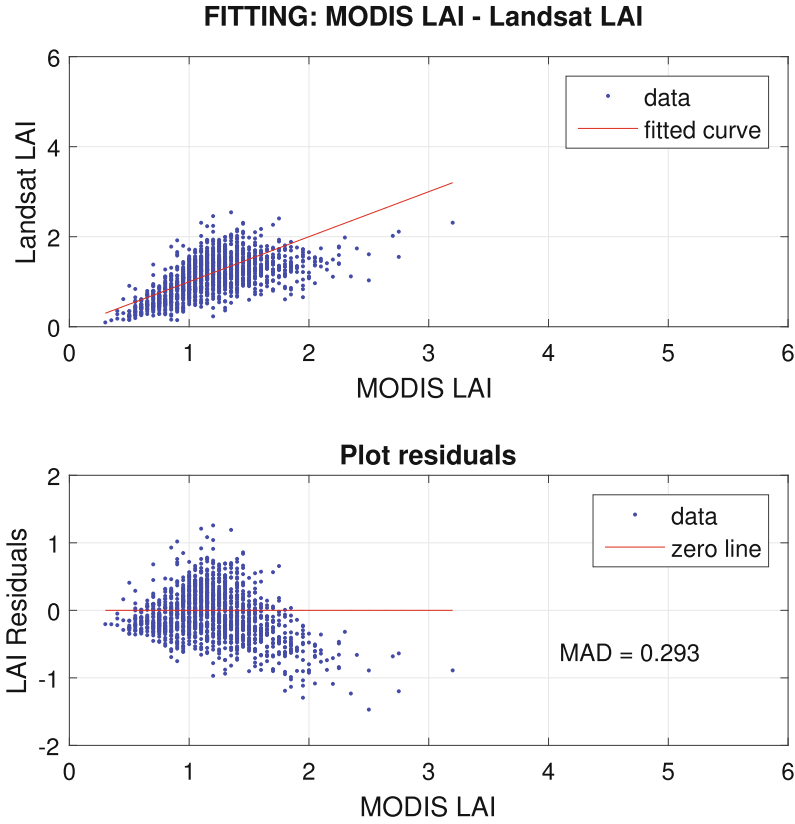


Fig. 2. Scatter plot between LAI MODIS and LAI Landsat retrieved using the CLAIR model and aggregated to the MODIS pixel resolution for the surface reflectance acquisition of the 07/13/2013 (DOY 194).

It globally ranges from 0.12 and 0.30 with a mean value of 0.23. The MAD results, between Landsat retrievals and MODIS LAI products, are in lines with the ones showed by Gao et al. [2]. They found MAD values in the range 0.07–0.80 for the High-Quality MODIS LAI pixels used as training sample.

Moreover, for each scene was analyzed the distribution of LAI values retrieved using the two sets of parameters. Figure 3 shows the histogram related to the scene with the highest WDV_I value found (0.61). This condition was selected since it highlights LAI saturation problems. The histograms show that by adopting a WDV_I_∞ values major than the maximum one, the distribution of LAI remains the same whereas the differences, in terms of MAD, are non-significant. The most important consequence is that the maximum LAI value retrieved within the image ranges from 20.79 to 8.42. However, this occurs for a very little number of saturated pixels. In this way is possible to reduce LAI saturation problems and further extend the future application of the model for the newly images.

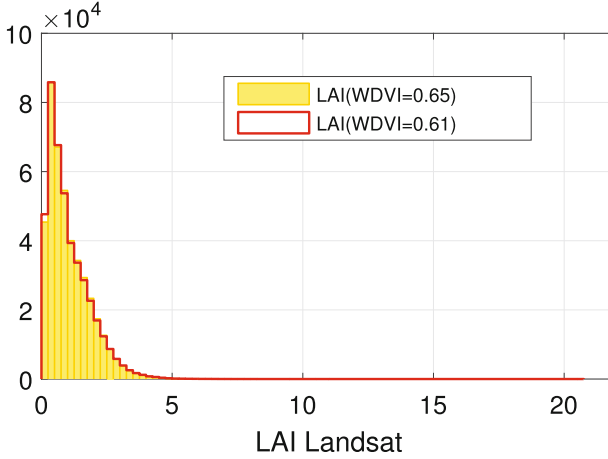


Fig. 3. Histogram (bin width equal to 0.25) of LAI related to the maximum WDVl values for the entire season (06/20/2013). The histogram considers only vegetated areas.

5 Conclusion

This study proposes an image-based method for the calibration of the CLAIR model using Landsat 8 surface reflectance data and MCD15A3H LAI products as reference. The proposed procedure generates reliable LAI information with a higher spatial resolution than LAI data used as reference. In this way, LAI information retrieved are suitable as input in large variety of climates, ecological and agricultural applications (e.g. crop yield prediction, evapotranspiration estimation). The procedure can be applied in case of lacking both LAI and surface reflectance field measurements and moreover it is not required the knowledge of crops present in the investigated area. In fact, the estimated parameters of the model can be considered site specific (and not crop specific) because during the calibration procedure were considered the mixture of all crop types present in the selected area. For its characteristics, image-based calibration represents a valid solution to extend the field of application of the CLAIR model.

The method was tested and statistically assessed in a territory of the irrigation district Sinistra Ofanto (Apulia region - Italy). Despite the extremely heterogeneous and fragmented landscape of the study area, the obtained results depict that, once calibrated, the CLAIR model is able to produce results conform to the MODIS data. In fact, MAD values were close to the range of MODIS LAI retrieval accuracy over all the considered scenes. Furthermore, the proposed calibration procedure can be furtherly tested by using others surface reflectance (e.g. Sentinel products) and LAI datasets.

References

1. Chen, J.M., Black, T.: Defining leaf area index for non-flat leaves. *Plant, Cell Environ.* **15**(4), 421–429 (1992)
2. Gao, F., Anderson, M.C., Kustas, W.P., Wang, Y.: Simple method for retrieving leaf area index from landsat using modis leaf area index products as reference. *J. Appl. Remote Sens.* **6**(1), 063554–1 (2012)
3. Duchemin, B., Hadria, R., Erraki, S., Boulet, G., Maisongrande, P., Chehbouni, A., Escadafal, R., Ezzahar, J., Hoedjes, J., Kharrou, M., et al.: Monitoring wheat phenology and irrigation in central Morocco: on the use of relationships between evapotranspiration, crops coefficients, leaf area index and remotely-sensed vegetation indices. *Agric. Water Manag.* **79**(1), 1–27 (2006)
4. Anderson, M.C., Kustas, W.P., Norman, J.M., Hain, C.R., Mecikalski, J.R., Schultz, L., González-Dugo, M.P., Cammalleri, C., d’Urso, G., Pimstein, A., Gao, F.: Mapping daily evapotranspiration at field to continental scales using geostationary and polar orbiting satellite imagery. *Hydrol. Earth Syst. Sci.* **15**(1), 223–239 (2011)
5. Jégo, G., Pattey, E., Liu, J.: Using leaf area index, retrieved from optical imagery, in the stics crop model for predicting yield and biomass of field crops. *Field Crops Res.* **131**, 63–74 (2012)
6. Bréda, N.J.: Ground-based measurements of leaf area index: a review of methods, instruments and current controversies. *J. Exp. Bot.* **54**(392), 2403–2417 (2003)
7. Martinez, B., Cassiraga, E., Camacho, F., Garcia-Haro, J.: Geostatistics for mapping leaf area index over a cropland landscape: efficiency sampling assessment. *Remote Sens.* **2**(11), 2584–2606 (2010)
8. Tarantino, E., Figorito, B.: Extracting buildings from true color stereo aerial images using a decision making strategy. *Remote Sens.* **3**(8), 1553–1567 (2011)
9. Richter, K., Vuolob, F., D’Urso, G., Dini, L.: Evaluation of different methods for the retrieval of LAI using high resolution airborne data. In: *Proceedings of SPIE, the International Society for Optical Engineering, Society of Photo-Optical Instrumentation Engineers*, p. 67420E–1 (2007)
10. Verrelst, J., Rivera, J.P., Veroustraete, F., Muñoz-Marí, J., Clevers, J.G., Camps-Valls, G., Moreno, J.: Experimental sentinel-2 LAI estimation using parametric, non-parametric and physical retrieval methods-a comparison. *ISPRS J. Photogramm. Remote Sens.* **108**, 260–272 (2015)
11. Balacco, G., Figorito, B., Tarantino, E., Gioia, A., Iacobellis, V.: Space-time lai variability in Northern Puglia (Italy) from spot vgt data. *Environ. Monit. Assess.* **187**(7), 434 (2015)
12. Clevers, J.: Application of a weighted infrared-red vegetation index for estimating leaf area index by correcting for soil moisture. *Remote Sens. Environ.* **29**(1), 25–37 (1989)
13. Clevers, J.: The derivation of a simplified reflectance model for the estimation of leaf area index. *Remote Sens. Environ.* **25**(1), 53–69 (1988)
14. Baret, F., Jacquemoud, S., Hanocq, J.: The soil line concept in remote sensing. *Remote Sens. Rev.* **7**(1), 65–82 (1993)
15. Vanino, S., Nino, P., De Michele, C., Bolognesi, S.F., Pulighe, G.: Earth observation for improving irrigation water management: a case-study from Apulia region in Italy. *Agric. Agric. Sci. Proc.* **4**, 99–107 (2015)

16. Vuolo, F., Neugebauer, N., Bolognesi, S.F., Atzberger, C., D'Urso, G.: Estimation of leaf area index using Deimos-1 data: application and transferability of a semi-empirical relationship between two agricultural areas. *Remote Sens.* **5**(3), 1274–1291 (2013)
17. Clevers, J.: Application of the WDVl in estimating LAI at the generative stage of barley. *ISPRS J. Photogramm. Remote Sens.* **46**(1), 37–47 (1991)
18. Novelli, A., Tarantino, E., Fratino, U., Iacobellis, V., Romano, G., Gentile, F.: A data fusion algorithm based on the Kalman filter to estimate leaf area index evolution in durum wheat by using field measurements and modis surface reflectance data. *Remote Sens. Lett.* **7**(5), 476–484 (2016)
19. Novelli, A.: A data fusion kalman filter algorithm to estimate leaf area index evolution by using Modis LAI and PROBA-V top of canopy synthesis data. In: Fourth International Conference on Remote Sensing and Geoinformation of the Environment. International Society for Optics and Photonics (2016). 968813
20. Clevers, J., Vonder, O., Jongschaap, R., Desprats, J.F., King, C., Prévot, L., Bruguier, N.: Using spot data for calibrating a wheat growth model under mediterranean conditions. *Agronomie* **22**(6), 687–694 (2002)
21. Apollonio, C., Balacco, G., Novelli, A., Tarantino, E., Piccinni, A.F.: Land use change impact on flooding areas: the case study of Cervaro Basin (Italy). *Sustainability* **8**(10), 996 (2016)
22. Novelli, A., Tarantino, E., Caradonna, G., Apollonio, C., Balacco, Gabriella, Piccinni, Ferruccio: Improving the ANN classification accuracy of landsat data through spectral indices and linear transformations (PCA and TCT) aimed at LU/LC monitoring of a river basin. In: Gervasi, O., et al. (eds.) ICCSA 2016. LNCS, vol. 9787, pp. 420–432. Springer, Cham (2016). doi:[10.1007/978-3-319-42108-7_32](https://doi.org/10.1007/978-3-319-42108-7_32)
23. Clevers, J., Vonder, O., Jongschaap, R., Desprats, J., King, C., Prévot, L., Bruguier, N.: A semi-empirical approach for estimating plant parameters within the reseda-project. *Int. Archives Photogramm. Remote Sens.* **33**, 272–279 (2000). B7/1; Part 7
24. Vuolo, F., Dini, L., D'Urso, G.: Assessment of LAI retrieval accuracy by inverting a RT model and a simple empirical model with multiangular and hyperspectral CHRIS/PROBA data from SPARC. In: Proceedings of the 3rd CHRIS/Proba Workshop (2005)
25. Minacapilli, M., Iovino, M., D'Urso, G., Osann Jochum, M., Moreno, J.: Crop and irrigation water management using high resolution remote sensing and agrohydrological models. In: AIP Conference Proceedings, vol. 852, pp. 99–106. AIP (2006)
26. Neugebauer, N., Vuolo, F.: Crop water requirements on regional level using remote sensing data—a case study in the marchfeld region berechnung des pflanzenwasserbedarfs für sommerfeldfrüchte mittels fernerkundungsdaten. eine fallstudie in der marchfeld-region. *Photogramm. Fernerkund. Geoinf.* **2014**(5), 369–381 (2014)
27. Yoshioka, H., Miura, T., Demattê, J.A., Batchily, K., Huete, A.R.: Soil line influences on two-band vegetation indices and vegetation isolines: a numerical study. *Remote Sens.* **2**(2), 545–561 (2010)
28. Balenzano, A., Satalino, G., Lovergine, F., Rinaldi, M., Iacobellis, V., Mastronardi, N., Mattia, F.: On the use of temporal series of L-and X-band SAR data for soil moisture retrieval. capitanata plain case study. *Eur. J. Remote Sens.* **46**(1), 721–737 (2013)
29. Aquilino, M., Novelli, A., Tarantino, E., Iacobellis, V., Gentile, F.: Evaluating the potential of geoeye data in retrieving LAI at watershed scale. In: SPIE Remote Sensing. International Society for Optics and Photonics (2014). 92392B–92392B

30. Tarantino, E., Novelli, A., Laterza, M., Gioia, A.: Testing high spatial resolution worldview-2 imagery for retrieving the leaf area index. In: Third International Conference on Remote Sensing and Geoinformation of the Environment. International Society for Optics and Photonics (2015). 95351N
31. Akdim, N., Alfieri, S.M., Habib, A., Choukri, A., Cheruiyot, E., Labbassi, K., Menenti, M.: Monitoring of irrigation schemes by remote sensing: phenology versus retrieval of biophysical variables. *Remote Sens.* **6**(6), 5815–5851 (2014)
32. Vanino, S., Pulighe, G., Nino, P., De Michele, C., Bolognesi, S.F., D’Urso, G.: Estimation of evapotranspiration and crop coefficients of tendone vineyards using multi-sensor remote sensing data in a mediterranean environment. *Remote Sens.* **7**(11), 14708–14730 (2015)
33. Giordano, R., Milella, P., Portoghese, I., Vurro, M., Apollonio, C., D’Agostino, D., Lamaddalena, N., Scardigno, A., Piccinni, A.: An innovative monitoring system for sustainable management of groundwater resources: objectives, stakeholder acceptability and implementation strategy. In: 2010 IEEE Workshop on Environmental Energy and Structural Monitoring Systems (EESMS), pp. 32–37. IEEE (2010)
34. Giordano, R., D’Agostino, D., Apollonio, C., Scardigno, A., Pagano, A., Portoghese, I., Lamaddalena, N., Piccinni, A.F., Vurro, M.: Evaluating acceptability of groundwater protection measures under different agricultural policies. *Agric. Water Manag.* **147**, 54–66 (2015)
35. Vermote, E., Justice, C., Claverie, M., Franch, B.: Preliminary analysis of the performance of the landsat 8/OLI land surface reflectance product. *Remote Sens. Environ.* **185**, 46–56 (2016)
36. Roy, D.P., Wulder, M., Loveland, T., Woodcock, C., Allen, R., Anderson, M., Helder, D., Irons, J., Johnson, D., Kennedy, R., et al.: Landsat-8: science and product vision for terrestrial global change research. *Remote Sens. Environ.* **145**, 154–172 (2014)
37. Knyazikhin, Y., Glassy, J., Privette, J., Tian, Y., Lotsch, A., Zhang, Y., Wang, Y., Morisette, J., Votava, P., Myneni, R., et al.: Modis leaf area index (LAI) and fraction of photosynthetically active radiation absorbed by vegetation (FPAR) product (MOD15) algorithm theoretical basis document. Theoretical Basis Document. NASA Goddard Space Flight Center, Greenbelt, MD 20771 (1999)
38. Yang, W., Shabanov, N., Huang, D., Wang, W., Dickinson, R., Nemani, R., Knyazikhin, Y., Myneni, R.: Analysis of leaf area index products from combination of modis terra and aqua data. *Remote Sens. Environ.* **104**(3), 297–312 (2006)
39. Weier, J., Herring, D.: Measuring Vegetation (NDVI & EVI) (2011)
40. D’Urso, G.: Simulation and Management of On-Demand Irrigation Systems: A Combined Agrological and Remote Sensing Approach [sn] (2001)

Computational Science and Its Applications – ICCSA
2017

17th International Conference, Trieste, Italy, July 3-6,
2017, Proceedings, Part IV

Gervasi, O.; Murgante, B.; Misra, S.; Borruso, G.; Torre,
C.M.; Rocha, A.M.A.C.; Tanir, D.; Apduhan, B.O.;
Stankova, E.; Cuzzocrea, A. (Eds.)

2017, XXXVI, 749 p. 409 illus., Softcover

ISBN: 978-3-319-62400-6